Chemical Science

Controlled synthesis of organic two-dimensional nanostructures *via* reaction-driven, cooperative supramolecular polymerization†

Shikha Dhiman, [ID] ‡ Rita Ghosh,‡§ Souvik Sarkar and Subi J. George [ID] *

The bottom-up approach of supramolecular polymerization is an effective synthetic method for functional organic nanostructures. However, the uncontrolled growth and polydisperse structural outcome often lead to low functional efficiency. Thus, precise control over the structural characteristics of supramolecular polymers is the current scientific hurdle. Research so far has tended to focus on systems with inherent kinetic control by the presence of metastable state monomers either through conformational molecular design or by exploring pathway complexity. The need of the hour is to create generic strategies for dormant states of monomers that can be extended to different molecules and various structural organizations and dimensions. Here we venture to demonstrate chemical reaction-driven cooperative supramolecular polymerization as an alternative strategy for the controlled synthesis of organic two-dimensional nanostructures. In our approach, the dynamic imine bond is exploited to convert a non-assembling dormant monomer to an activated amphiphilic structure in a kinetically controlled manner. The chemical reaction governed retarded nucleation–elongation growth provides control over dispersity and size.

Introduction

Organic two-dimensional (2D) nanostructures[1] composed of semiconducting π-conjugated molecules are important for various optoelectronic applications.[2,3] The bottom-up approach of self-assembly has been proven to be an effective synthetic method for the synthesis of defect-free 2D-nanosheets by the well-ordered organization of organic π-conjugated amphiphiles.[4] The structural control over the size and dispersity of these 2D organic nanostructures is crucial for their functional outcome.[3] However, the controlled growth of organic monomers in two-dimensions has been a challenge and is seldom reported.[5] In a pioneering study, crystallization-driven self-assembly[6] (CDSA) has been employed to control the micellar organization of block copolymer amphiphiles to construct precision 2D nanostructures.[7]

In this context, the structural control of one-dimensional organic nanostructures has been recently realized by living supramolecular polymerization (LSP).[8] The strategy involves

kinetic control over the nucleation or initiation phase during the nucleation-growth supramolecular polymerization to prevent spontaneous growth.[9] In a unique strategy, a conformationally inactive metastable monomeric state[10] was utilized for initiator-mediated chain-growth[11] supramolecular polymerization. Alternatively, the most common design involves the kinetic trapping of monomers in non-equilibrium metastable aggregated states[12] by exploiting the pathway complexity[13] to realize seed-induced LSP. Sugiyasu and co-workers recently extended the seeded approach for the synthesis of 2D supramolecular polymers with a controlled area and narrow dispersity.[14]

In an attempt to generalize the design of LSP and to make it independent of the monomer structure, we have established the concept of dormant monomers in fuel or chemical reaction-driven LSP.[15] In this bioinspired approach, the kinetics of the reaction, which can be modulated by external molecular cues, determine the rate of supramolecular polymerization.[16,17] This strategy comprises a dormant monomer which, unlike the above-mentioned metastable dormant state, due to its thermodynamic stability, does not undergo self-assembly on its own (Scheme 1a). Hence, an external cue, an activator, is essential to *in situ* convert the non-assembling dormant monomer to an assembling active monomer which undergoes kinetically controlled, cooperative supramolecular polymerization.[16] As a consequence, the activation step (k_A) would be the rate-determining step (R.D.S.) and hence both the extent and kinetics of the self-assembly process can be directly modulated

Supramolecular Chemistry Laboratory, New Chemistry Unit, School of Advanced Materials (SAMat), Jawaharlal Nehru Centre of Advanced Scientific Research (JNCASR), Jakkur, Bangalore 560064, India. E-mail: george@jncasr.ac.in; subijg@gmail.com

† Electronic supplementary information (ESI) available. See DOI: 10.1039/d0sc02670k

‡ Both the authors contributed equally.

§ Current affiliation: Department of Chemistry, St. Joseph's College (Autonomous), Bangalore, India.
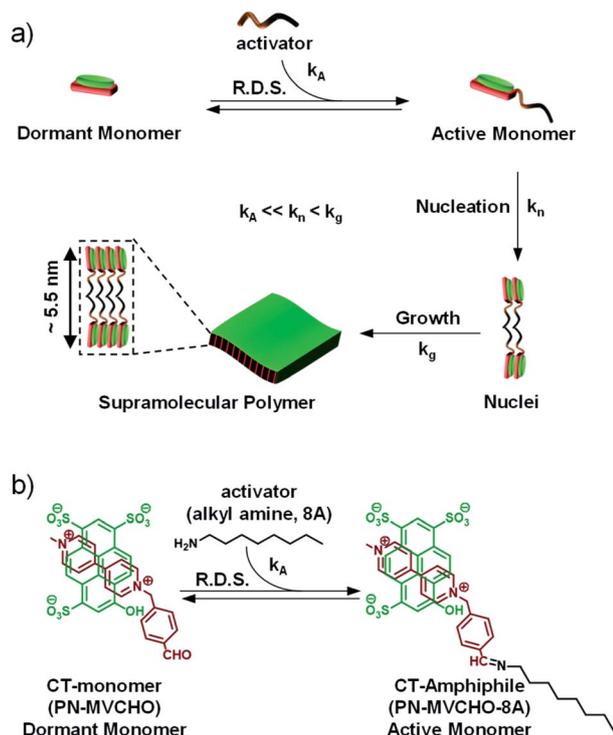
Scheme 1 (a) Schematic illustration of the chemical reaction (imine bond)-driven activation of a dormant monomer (charge-transfer (CT)-monomer) to an active monomer (CT-amphiphile) by an activator which further undergoes nucleation-growth into bilayer sheets. (b) Chemical structure and reaction for the activation of a CT-complex composed of a pyranine (**PN**) donor and methyl viologen benzaldehyde (**MVCHO**) acceptor to the CT-amphiphile by octyl amine (**8A**). k_A = rate of activation, k_n = rate of nucleation, k_g = rate of growth/elongation and R.D.S. = rate determining step.

by the concentration of the activator. This was demonstrated recently by our group to attain complete control over the structural and temporal features of 1D supramolecular polymers.[17] So far the fuel-driven strategy has only been applied to 1-dimensional (1D) nanostructures. However, controlled synthesis of 2D nanostructures has immense importance in organic materials, as mentioned above.

Herein we report the generic nature of the chemical reaction-driven cooperative supramolecular approach for the controlled synthesis of 2D nanostructures from organic semiconducting monomers, which can be modulated by variation of the concentration of molecular cues for a controlled dispersity and size.

Design strategy

Charge-transfer (CT) supramolecular amphiphiles, with donor (D) and acceptor (A) π-stacked components, were extensively studied by Zhang's group and by our group independently to create semiconducting alternating supramolecular polymers in various dimensions for their optoelectronic and stimuli-responsive applications.[18] However, due to spontaneous self-assembly (Scheme 1, k_n and k_g are high), they lack controlled

dimensions, and thus there is high scope to increase their functional efficiency. For this, kinetic regulation ($k_A \ll k_n$) over the supramolecular polymerization process is required that can retard the nucleation process.[19] However, the strategy of kinetic trapping of monomers *via* an off-nucleation pathway or conformational metastable state cannot be applied in these systems as most of the CT supramolecular monomers are highly dynamic and fall spontaneously into thermodynamic equilibrium. Therefore, in our approach to realizing kinetically controlled supramolecular polymerization, we designed a dormant monomer state comprising an oppositely charged D and A that form the CT-complex (**PN-MVCHO**).

Since the CT-complex, **PN-MVCHO** (dormant CT-monomer), is charged, it remains well-dispersed in aqueous solution as a discrete, non-covalent monomer and lacks any propensity to aggregate (Scheme 1). Moreover, the aldehyde group appended to the acceptor acts as the reactive center for the nucleophilic reaction of amine to form the dynamic imine bond.[20] As a consequence, the imine reaction orchestrates the conversion of the dormant CT-monomers to the active monomeric state (**PN-MVCHO-8A**, k_A, Scheme 1), with a non-covalent amphiphile structure, in a temporal manner that governs the kinetically controlled supramolecular polymerization process and hence is the rate-determining step (R.D.S.). Further, the kinetics and extent of this chemical reaction-driven supramolecular polymerization can be modulated by the change in reactivity (by changing the pH) or the concentration of the substrates, amine (**8A**) in the present case.

Results and discussion

Packing factor calculation for two-dimensional supramolecular assembly

We aim to construct a two-dimensional supramolecular assembly of non-covalent CT-amphiphilic monomers, with controlled dispersity and size. Amphiphilic systems are highly designable with a predictable morphological outcome. Hence, to predict the nanostructure morphology, we have calculated the packing factor of the supramolecular CT-amphiphile using the Tanford equation.[21] In our previous study, we employed the CT-amphiphile with coronene tetra potassium salt (**CS**) as the donor component and the imine adduct of octyl amine (**8A**) and methyl viologen benzaldehyde (**MVCHO**) as the acceptor component.[17] The resultant supramolecular CT-amphiphile (**CS-MVCHO-8A**) with a head size of 7.5 Å and a tail size of 11.62 Å yielded a packing factor of 0.47 corresponding to a cylindrical micellar arrangement (see the ESI†). The calculation is in agreement with the experimentally observed one-dimensional nanostructures with micellar packing of the amphiphilic CT-monomers.[17]

On the other hand, a two-dimensional (2D) bilayer organization demands a packing factor of 0.9–1.0 according to the Tanford equation. To increase the packing factor, the interfacial area and head size of the amphiphile should be decreased to half that for the **CS-MVCHO-8A**, *i.e.* ~3.75 Å. Keeping this in mind, in the present study, we have replaced the **CS** with a smaller pyranine donor molecule, **PN**, and used the same

acceptor component. As a result, the head group size decreases, and a resultant packing factor of 0.91 is obtained. Hence we envisage that the bilayer assembly of non-covalent **PN-MVCHO-8A** amphiphilic monomers would yield bilayer 2D sheets.

Imine reaction-driven 2D supramolecular polymerization

We aim to control the structural properties of 2D assemblies via kinetically controlled growth, mediated by the chemical reaction, herein the imine reaction. The imine reaction-driven kinetics of self-assembly would depend on three factors (Scheme 1). Firstly, the reactivity of the amine to convert the CT-complex to the CT-amphiphile via the imine reaction. Secondly, the thermodynamic stability of the end product, herein CT self-assembly, shifts the dynamic reaction equilibrium towards the aggregated state and thus amine is further consumed. The third is the concentration of amine that influences both the above-stated factors.

Before the self-assembly study, we investigated the formation and stoichiometry of the D and A components in the inactive CT-monomer. A 1 : 1 stoichiometry of **PN** (donor) and **MVCHO** (acceptor) in the CT-monomer was calculated from the titration curve where a charge-transfer induced quenching of **PN** emission (λ_{ex} = 350 nm) and appearance of a new CT-absorption band around 550–650 nm in a 5×10^{-4} M aqueous solution are observed (Fig. S1a and S2†). The concentration dependent absorption study of the CT complex shows a linear change in the CT absorption band, i.e. it follows the Lambert–Beer law in the concentration regime of 1×10^{-3} to 8×10^{-5} M (Fig. S3†). This suggests that the molecule does not undergo any assembly–disassembly phenomenon and a mere change of its concentration occurs. Further absence of scattering at higher wavelength confirms that the non-covalent CT-monomer is highly soluble in water and has no propensity to self-assemble in an alkaline solution.

Next, we investigated the imine-driven supramolecular polymerization to a controlled extent. Since CT-interaction is known to get enhanced with self-assembly, we believed that the conversion of the CT-monomer to the CT-amphiphile and subsequent self-assembly can be probed by the increase in the CT-absorption band and a further quenching of **PN** emission (Fig. S4†). To investigate this, 1 equivalent (eq.) of octyl amine (**8A**) was added to an aqueous solution of 5×10^{-4} M **PN-MVCHO** at pH 11.5, and the spectral properties were probed after 2 hours of incubation. As the reactivity of amine determines the kinetics of the imine reaction, we kept the pH alkaline at ca. 11.5, which ensures that the deprotonated form of **8A** exhibits high nucleophilicity. After the incubation time, an enhancement in the CT-absorption band along with a further quenching in **PN** emission was observed for **PN-MVCHO-8A** in comparison with the inactive CT monomer, **PN-MVCHO**, solution (Fig. S4†). The formation of self-assembled structures in solution is reiterated by the increase in size from 220 to 620 nm observed by dynamic light scattering (DLS) measurements (Fig. S5†).

The strengthening of the CT-interaction on amphiphilicity-driven self-assembly was further proven by the increase in the association constant (K_a) between the donor and acceptor from 1.7×10^5 M for the CT-monomer (**PN-MVCHO**) to 3.6×10^5 M

for the CT-amphiphile (**PN-MVCHO-8A**) by fitting their emission titration curves to a 1 : 1 binding model (Fig. S1†). As the CT strength is also determined by the distance between the D and A components, the amphiphilicity-driven self-assembly further strengthens the existing CT-interaction in monomers.

To confirm that the observed self-assembly is indeed driven by the imine formation, ^{1}H NMR was performed to quantify the imine reaction by monitoring the consumption of **MVCHO** through the protons of its aldehyde functional group. The ^{1}H NMR of **PN-MVCHO** in D$_2$O at pH 11.5 with 1 eq. of an internal standard of sodium acetate was first recorded (Fig. S6a and b†). To the same solution, 1 eq. of **8A** in D$_2$O was added and after 2 hours of incubation NMR was recorded. The ^{1}H NMR spectrum shows complete disappearance of the aldehyde peak and broadening of other peaks suggesting 100% imine formation to promote self-assembly (Fig. S6a†). This depicts the interdependency of imine-driven self-assembly and the shifts of the dynamic imine reaction equilibrium due to the thermodynamic stability of CT self-assembly.[17]

As discussed earlier, most of the CT-based assemblies reported in the literature are highly dynamic and fall instantaneously to the thermodynamic minimum and thus lack any kinetic control over their supramolecular polymerization process.[18] Similarly, the CT formation is very fast in the present system and we envisage that the kinetics of the formation of imine should be the rate determining step in the growth process (Scheme 1). To investigate this, the change in absorbance on the formation of CT extended assembly from inactive CT-monomers was probed during the growth process. For this, a solution of 5×10^{-4} M **PN-MVCHO** at pH 11.5 was taken and to it 1 eq. of **8A** was added and the time-dependent absorbance changes at 670 nm (characteristic of CT) were monitored. The kinetic experiment revealed a non-linear increase in absorbance saturating at ~2000 seconds (Fig. 1a). The changes in the absorbance could be due to the combined effect of an increase in the CT absorption and the increased scattering upon the self-assembly process. However, the kinetics monitored via light scattering which exclusively probes the growth process matches well with absorbance kinetics, suggesting that spectroscopic changes indeed probe the growth process. As the inactive CT-monomer has no inherent kinetics of growth, the kinetics observed is attributed to the rate of formation of imine.

Thus the spectroscopic probing of the growth process suggests a kinetically controlled supramolecular polymerization by imine-reaction triggered self-assembly. Hence we next investigated its effect on the structural characteristics of the supramolecular polymer thus obtained. The morphological outcome of **PN-MVCHO-8A** self-assembly was investigated through transmission electron microscopy (TEM) which displayed the formed 2D sheets with >1 μm size (Fig. 1b and S7†) is consistent with the prediction from the packing factor. Atomic Force Microscopy (AFM) also showed thin sheets of a 5.5 nm height, revealing a non-interdigitated bilayer packing of the supramolecular amphiphile, **PN-MVCHO-8A**, along the thickness of the sheets, as calculated from the energy minimized structure (Fig. S8†). Zeta potential measurements suggest a negatively charged surface (−37 mV) of the sheets due to the
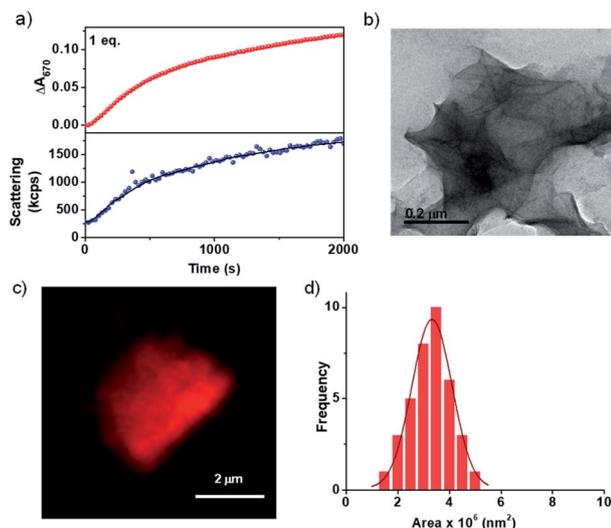
Fig. 1 (a) Probing the growth of the **PN-MVCHO-8A** assembly *via* the time-dependent changes in absorbance at 670 nm and *via* scattering changes (monitored *via* DLS) showing a similar trend in growth with 1.0 eq. **8A**. (b) TEM image and (c) confocal image (Nile red encapsulated in the hydrophobic bilayer) of the **PN-MVCHO-8A** assembly showing the formation of 2D sheets. [Nile red] = 1×10^{-6} M. (d) Area distribution profile obtained from confocal microscopy images depicting a controlled PDI of 1.06. [**PN**] = [**MVCHO**] = [**8A**] = 5×10^{-4} M, pH = 11.5.

dominance of anionic groups of **PN-MVCHO** (trianionic **PN** *versus* dicationic **MVCHO**) on the surface, which helps to obtain the single-layered sheets due to electrostatic repulsion (Fig. S9†). To confirm the bilayer packing, a polarity responsive hydrophobic dye, Nile red, was used to stain the sheets. Confocal fluorescence microscopy images show the formation of 2D sheets in solution imaged using Nile red dye encapsulation in the hydrophobic pockets of the nanostructures, which also allowed the visualization of 2D nanostructures in the solution phase without any solvent drying effects (Fig. 1c). Statistical analyses of these fluorescent 2D nanostructures revealed an average surface area of 3.3×10^{6} nm^2 with a narrow polydispersity index (PDI) of 1.06 (Fig. 1d and S10†). Thus it is evident that the imine reaction drives the conversion of the dormant monomer to the active monomer that undergoes kinetically controlled supramolecular polymerization into well-defined 2D sheets with a bilayer organization.

To further investigate the primary factor which is the effect of reactivity of the amine on the kinetics of self-assembly, the nucleophilicity of the amines is altered. Amines with high nucleophilicity are expected to undergo fast imine formation whereas protonated amines would not have any propensity towards imine formation. To scrutinize imine-assisted supramolecular polymerization, first, pH-dependence on the extent of imine formation is studied by ^{1}H NMR spectroscopy. The ^{1}H NMR spectra of **PN-MVCHO** with and without **8A** were measured at pH 7 and 10 (Fig. S6c and d†). Integration with respect to the internal standard sodium acetate revealed 8% and 37% aldehyde consumption, respectively, in the presence of **8A** (Fig. S6e†). Thus, at lower pH, the extent of imine formation

is low due to lower nucleophilicity of the amine. This influence of pH on the chemical reaction also directly influences the rate and extent of self-assembly as elucidated by the absorption kinetic profiles. At pH 7, no growth occurs whereas at pH 10 there is sigmoidal growth but the rate and extent of self-assembly are too low compared to those at pH 11.5 (keeping the concentration of all other components constant) as evident from the absorption kinetics (Fig. S11†).

Hence, this proves that our strategy of chemical reaction-driven supramolecular polymerization provides a tool to modulate the extent of self-assembly and its kinetics by altering the reactivity of the amine which could be controlled by an external cue, pH in this case.

Chemical reaction-driven, cooperative supramolecular polymerization

An important characteristic of chemical reaction-driven self-assembly is the possible modulation of the rate of the reaction and hence the growth by variation of the external cues such as pH (*vide supra*) or concentration of substrates. Here we explore the effect of the change in the initial concentration of amine on the rate of the imine reaction and subsequent growth of the supramolecular polymer as well as the extent of self-assembly (Fig. 2). In order to explore this, the amount of **8A** added to 5×10^{-4} M **PN-MVCHO** at pH 11.5 was varied from 0.2 eq. to 1.0 eq. and the corresponding absorbance changes at 670 nm were monitored for the growth process. The kinetics show a significant deceleration as the concentration of **8A** was decreased (Fig. 2b–d and S12†). A remarkable sigmoidal growth was observed depicting a cooperative mechanism of growth, which is confirmed by the good fit of the growth kinetics to Watzky–Finke's two-state nucleation-growth model (Fig. S13†). The nucleation rate constant (k_n) calculated for 0.3 eq. of **8A** was 2.3×10^{-5} s^{-1} in comparison to the 5.6×10^{-4} s^{-1} for 0.4 eq. of **8A** (Fig. 2b–d). Further, the growth kinetics acquired from the absorbance changes show a direct correlation with scattering confirming the changes monitored by absorbance are indeed due to growth (Fig. 2b and c).

In the case of 1 eq. of **8A**, non-sigmoidal kinetics with a half time (t_{50}) of 485 seconds with no lag phase was observed (Fig. 2d). However, lowering the concentration of amine to 0.3 eq. of **8A** resulted in sigmoidal growth with a t_{50} of 1700 seconds and a lag phase of *ca.* 165 seconds (Fig. 2d and S14†). Final intensity % size data show a dependence of size on the concentration of amine. For 0.3 eq. a size of 950 ± 130 nm, for 0.4 eq., 1280 ± 160 nm and for 0.5 eq., 1425 ± 120 nm were obtained indicating that a higher concentration of amine results in bigger assemblies (Fig. 2e and S7b†). As DLS assumes a spherical morphology and the present study deals with 2-dimensional assembly, DLS is only employed to provide a trend (qualitative analysis) of the size difference and we do not emphasize the exact numerical values (quantitative analysis).

To further investigate the growth process, the kinetic parameters obtained for 0.2–0.4 eq. were calculated as ≥0.5 eq. of **8A** do not exhibit any clear lag phase owing to fast kinetics (Fig. 2d and S13†). The kinetic parameters show an increase in
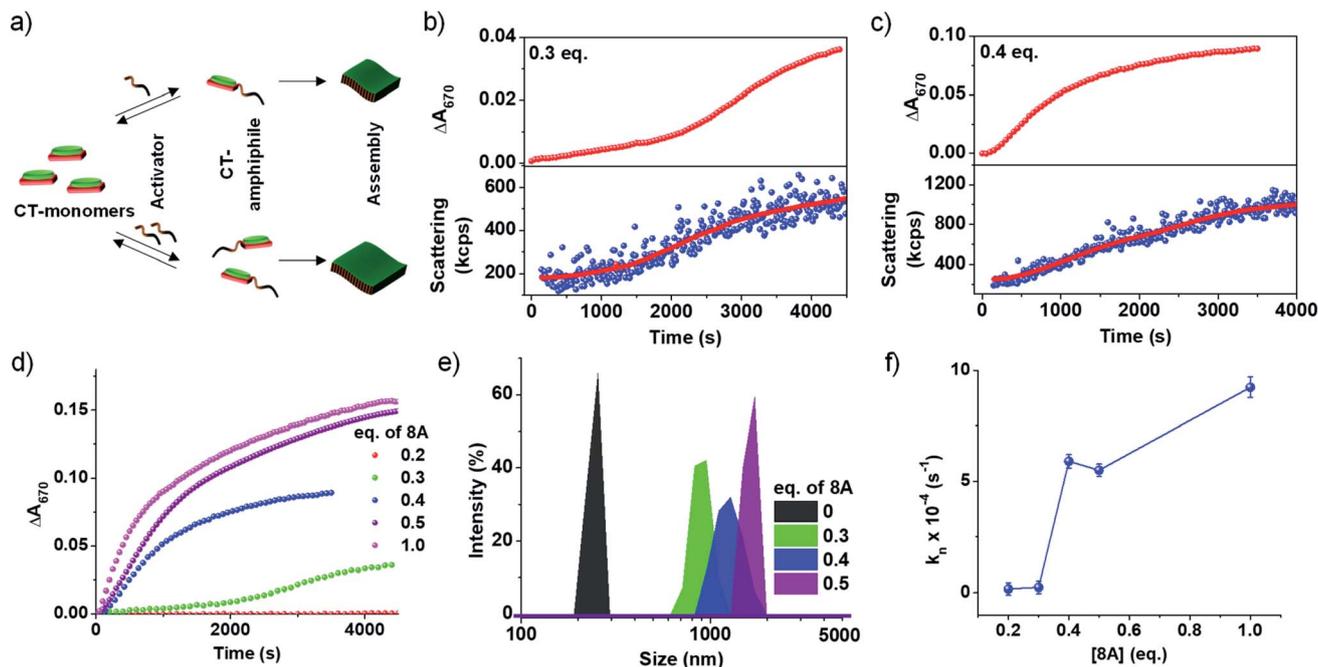
Fig. 2 Dependence of amine concentration [8A] on reaction driven 2D self-assembly of PN-MVCHO-8A. (a) Schematic representation of reaction-driven 2D self-assembly and its dependence on the concentration of amine (8A) used. Time-dependent changes in absorbance at 670 nm and scattering changes showing the effect of change in the concentration of 8A on the growth kinetics of the supramolecular polymer with (b) 0.3 eq. and (c) 0.4 eq. of 8A. (d) Time-dependent changes in absorbance at 670 nm with different concentrations of 8A. (e) DLS data showing the concentration of 8A dependent size of kinetically grown CT supramolecular polymers. (f) Effect of the nucleation rate (k_n) on 8A concentration. [PN] = [MVCHO] = 5×10^{-4} M, pH = 11.5.

the maximum rate (v_{max}) and a decrease in the halftime (t_{50}) and lag phase (t_{lag}) with an increase in the concentration of the activator (8A) (Fig. S14†). Further, the fitting of the kinetics to the Finke–Watzky model shows an increase in the nucleation rate (k_n) on increasing the 8A concentration (Fig. 2f and S13†). Since the kinetics of growth are determined by the reaction kinetics and monomer-assembly equilibrium, at low 8A concentration, the reaction is slow and hence the growth is less. At a higher 8A concentration, the reaction kinetics become fast and further autocatalyzed by the aggregation process. This results in the non-linear effect in the nucleation rate on increasing the 8A concentration (Fig. 2f).

Hence, the concentration of molecular cues, herein amine, can be utilized to directly affect the rate of imine formation and hence the growth of the supramolecular polymer which is not possible in other cooperative supramolecular assemblies where either solvent composition or temperature modulation is required to influence the energy landscape of the supramolecular polymerization process. This bioinspired strategy for chemical reaction-driven supramolecular polymerization is analogous to fuel-driven cooperative supramolecular polymerization in biological systems like actin.[16]

Chemical reaction-driven seeded supramolecular polymerization

The use of imine chemistry provides a remarkable control over the kinetics of self-assembly via a chemical reaction-driven

strategy. If the supramolecular polymerization undergoes a nucleation–elongation mechanism of growth and the nucleation step is well-retarded via slow kinetic control, it can exhibit seeded growth characteristics with a new batch of monomers. The in situ activated monomers in the present study can either grow independently via a homogeneous nucleation mechanism or grow on an existing assembly (referred to as a seed/nucleus) via heterogeneous nucleation. Amongst the two, the former occurs in a non-spontaneous nucleation process whereas the latter can spontaneously occur. Thus, activated monomers tend to choose the second pathway which is termed seeded supramolecular polymerization and which has been recently exploited to gain structural control of supramolecular polymers (Fig. 3). Further seeded supramolecular polymerization is a ubiquitous process in fuel-driven supramolecular assemblies in the biological realm.

Since the PN-MVCHO-8A system exhibits sigmoidal growth indicating a nucleation–elongation mechanism, we next investigate its seeding behavior. To investigate the seeded nature of reaction-driven self-assembly, we have introduced amines in batches (Fig. 3a) into a solution containing pre-grown assemblies and an excess of inactive dormant monomers, instead of a conventional seeding process where the seed is added to monomers trapped in a metastable state.[5] This method would ensure the in situ generation of active monomers in solution by the imine-reaction without undergoing any concentration dependent changes in the reaction equilibrium. Hence, we performed kinetically controlled growth by adding amine in
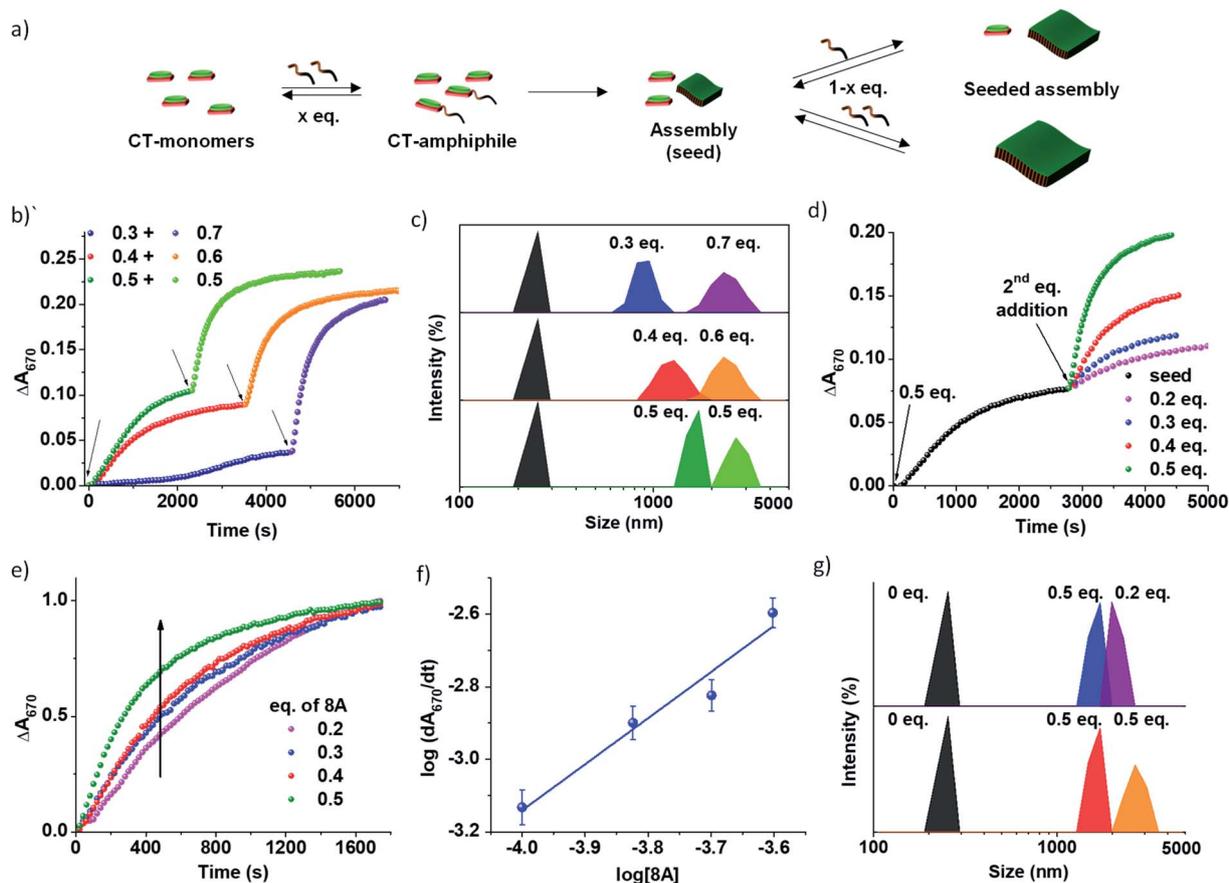
Fig. 3 Imine reaction driven seeded 2D self-assembly of **PN-MVCHO-8A**. (a) Schematic representation of seeded supramolecular assembly with addition of **8A** in batches. Temporal change in absorbance at 670 nm showing the initial sigmoidal kinetics for unseeded growth with subsequent non-sigmoidal kinetics on seeding (b) by adding **8A** in batches with the seed + monomer concentration kept constant with 1 eq. of **8A** and (d) constant seed (0.5 eq. **8A**) and variable monomer concentration (0.2–0.5 eq. **8A**). (c and g) DLS data showing a gradual increase in the size of the supramolecular assembly on seeding with the second batch of amine corresponding to the experiments in (b) and (d), respectively. (e) Normalized absorbance changes at 670 with time for seeding at a constant seed concentration depicting direct dependence of the rate of growth on the concentration of **8A**. (f) log–log plot of the rate of seeded growth with the concentration of active monomers (eq. of **8A**) at a constant seed concentration of 0.5 eq. $[\text{PN}] = [\text{MVCHO}] = 5 \times 10^{-4}$ M, pH = 11.5.

batches where its final concentration after the last addition is kept constant at 1.0 eq. For this, to a solution of 5×10^{-4} M **PN-MVCHO**, 0.3 eq. of **8A** was added and the time-dependent absorbance changes at 670 nm were monitored (Fig. 3a and b). Sigmoidal growth saturating at ~4560 seconds was observed with a nucleation rate of 2.3×10^{-5} s^{-1} (Fig. 3b). Addition of the remaining 0.7 eq. of **8A** to the same solution resulted in non-sigmoidal growth with a rate of 2.3×10^{-3} s^{-1} confirming the seeded growth of the *in situ* generated active monomers on the existing supramolecular polymer rather than formation of their independent nuclei (Fig. 3b).

Moreover, a similar trend was displayed when sequential additions of 0.4 + 0.6 eq. of **8A** and 0.5 + 0.5 eq. of **8A** were attempted. The DLS intensity % data suggested a gradual increase in size with the addition of the second batch of **8A** (Fig. 3c). In the case of 0.3 eq. of **8A**, an increase in size from 950 ± 400 nm to 2255 ± 130 nm is observed with the addition of 0.7 eq. of **8A**. Batch wise addition of 0.4 + 0.6 eq. of **8A** results in an increase in size from 1280 ± 365 nm to 2300 ± 160 nm. From

batch-wise addition of 0.5 eq. of **8A**, the first addition gives a 1430 ± 300 nm size and the second seeding gives a 2670 ± 120 nm size (Fig. 3b and S15a†). It is observed that the increase in the extent of growth with the second batch of addition is proportional to the concentration of amine introduced, is consistent with seeded assembly (Fig. 3b).[8]

Würthner and coworkers suggested that multicycle seeding is a mandatory requirement for the seeded supramolecular polymerization to exhibit living characteristics.[8] Hence, to explore the possibility of multicycle seeding, we added **8A** in three batches of 0.3 eq. each (Fig. S15b†). Similar to previous cases, the first growth was sigmoidal, whereas the second and third were non-sigmoidal with rates of 1.08×10^{-3} s^{-1} and 1.04×10^{-3} s^{-1}, respectively, reiterating seeded growth over multiple cycles of fuel addition (Fig. S15b†).

All the growth curves were non-sigmoidal depicting seeded kinetics. The increase in eq. of **8A** from 0.2 to 0.5 eq. resulted in an enhanced rate of seeded growth from 7×10^{-4} s^{-1} to 2.5×10^{-3} s^{-1} (Fig. S16†). Also, the amount of amine directly

determines the extent of self-assembly, which is evident from the seeding experiments with a fixed concentration of the seeds and with varying concentrations of amine **8A** for the second batch of addition (Fig. 3d). Interestingly, the plot of the log of the rate of seeded growth *versus* the log of the concentration of active monomers (eq. of **8A**) follows a linear increase which indicates the first-order rate of supramolecular polymerization with respect to amine and which along with non-sigmoidal growth validates a reaction-driven seeded growth (Fig. 3f). Further, the DLS intensity % data show a higher increase in size with higher eq. of the second batch of **8A** (Fig. 3g). Hence, the present system demonstrates chemical reaction-modulated kinetically controlled 2D supramolecular polymerization with seeded growth.

Controlled dispersity and size *via* seeded supramolecular polymerization

Kinetically controlled seeded growth aims to provide control over dispersity and size. Thus, it is necessary to scrutinize the dispersity and size obtained after the kinetic growth (Fig. 3). Although DLS gives a relative change in the size of aggregates upon the seeding process, it cannot be used as a probe to determine the polydispersity index (PDI) and the size of two-dimensional assemblies. Consequently, to probe the structural aspects of the two-dimensional nanostructures in solution, we have used confocal fluorescence microscopy. Since the nanosheets in their native state are non-fluorescent due to their CT character, an external polarity sensitive probe, Nile red, is used for their visualization as mentioned before, which exhibits a turn-on fluorescence when encapsulated in the bilayers of **PN-MVCHO-8A** sheets.

To further investigate the seeding characteristics of the **PN-MVCHO-8A** assembly, we added **8A** in two batches of 0.5 + 0.5 eq. in the presence of Nile red and attempted size analysis as in the previous case. Firstly, 0.5 eq. of **8A** was added and an average sheet area of $1.7 \pm 0.18 \times 10^6$ nm^2 with an aspect ratio of 1.10 and polydispersity index of 1.10 is observed (Fig. 4 and S17†). This is a smaller size compared to that obtained with 1 eq. confirming the amine-dependent degree of polymerization. Interestingly, on the addition of the second batch of 0.5 eq. of **8A**, an increase in size from $1.7 \pm 0.18 \times 10^6$ nm^2 to $3.5 \pm 0.05 \times 10^6$ nm^2, with approximately two times the area, is observed. However, PDI remained narrow (~1.10) with a negligible difference in the aspect ratio *i.e.* 1.13 (Fig. 4 and S18†). This substantiates that the imine bond directed kinetically controlled growth results in two-dimensional seeding of the CT monomers in a living manner (Scheme 1).

In order to get unequivocal proof of 2D seeded growth, Nile red was introduced only during the seeding process. Subsequent visualization confocal microscopy images revealed a frame-like structure with an inner unseeded dark region and outer fluorescent seeded region of **PN-MVCHO-8A** (Fig. S19†). Thus, indeed the chemical reaction-driven cooperative supramolecular polymerization provides an opportunity for kinetically controlled growth and seeded supramolecular polymerization for controlled size and dispersity. The difference
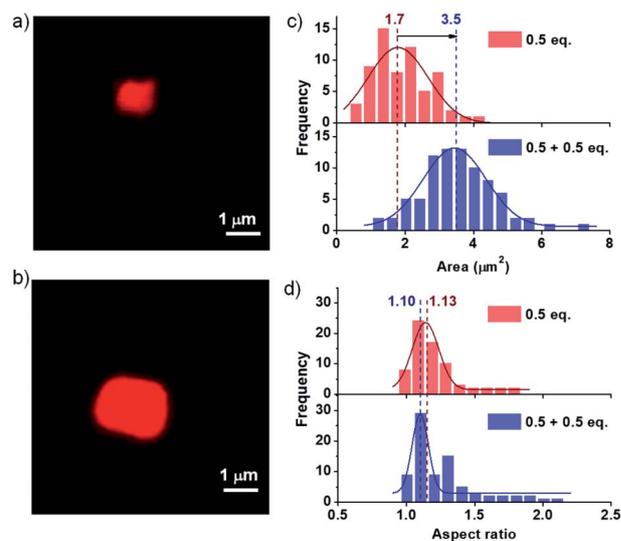

Fig. 4 Confocal microscopy images. (a) 0.5 eq. unseeded and (b) 0.5 eq. seeded on 0.5 eq. unseeded supramolecular assembly. The distribution profiles of (c) area and (d) aspect ratio obtained from confocal microscopy images depicting a controlled PDI and aspect ratio. [PN] = [MVCHO] = 5×10^{-4} M, pH = 11.5, [Nile red] = 1 µM.

in growth kinetics of previously studied **CS-MVCHO-8A** and **PN-MVCHO-8A** in the current work under the same reaction conditions indicated that self-assembly autocatalyzes the formation of imine bonds and hence plays an important role in determining the kinetics (Fig. S20†).

Conclusion

In conclusion, we demonstrated chemical reaction-driven controlled synthesis of 2D organic nanostructures composed of supramolecular CT-monomers. The study depicts the importance of chemical reaction-driven cooperative supramolecular polymerization as a generic strategy to achieve two fold-control over the growth process: first, the retarded nucleation step by the *in situ* kinetically controlled generation of active monomers for narrow dispersity, and secondly, the seeded supramolecular polymerization for a controlled size and aspect ratio. Moreover, the extent of supramolecular polymerization and the rate of growth could be controlled by external cues such as the concentration and reactivity of the substrate. We envisage that this strategy can be extended for precision supramolecular nanostructures in all dimensions, without the kinetic trapping of highly dynamic monomers in their metastable states. The strategy of dynamic covalent chemistry of imine can be applied to any amphiphilicity driven supramolecular polymerization and hence has a high substrate scope. Finally, a CT supramolecular assembly is highly programmable in terms of its dimensions by changing the size of the donor, acceptor, or alkyl tail which is not so predictable in other molecular assemblies. The aforementioned strategy also paves the way to construct radial organic heterostructures with fine microstructure control using multicomponent seeded supramolecular polymerization.[22]

Conflicts of interest

There are no conflicts to declare.

Acknowledgements

Notes and references

1 X. Zhuang, Y. Mai, D. Wu, F. Zhang and X. Feng, *Adv. Mater.*, 2015, **27**, 403–427; C. E. Boott, A. Nazemi and I. Manners, *Angew. Chem., Int. Ed.*, 2015, **54**, 13876–13894; B. Shen, Y. Kim and M. Lee, *Adv. Mater.*, 2020, 1905669; F. Ishiwari, Y. Shoji and T. Fukushima, *Chem. Sci.*, 2018, **9**, 2028; G. Wu, P. Verwilst, K. Liu, M. Smet, C. F. J. Faul and X. Zhang, *Chem. Sci.*, 2013, **4**, 4486–4493.

2 S. K. Park, J. H. Kim and S. Y. Park, *Adv. Mater.*, 2018, **30**, 1704759; F. Yang, S. Cheng, X. Zhang, X. Ren, R. Li, H. Dong and W. Hu, *Adv. Mater.*, 2018, **30**, 1702415; S. Ghosh, D. S. Philips, A. Saeki and A. Ajayaghosh, *Adv. Mater.*, 2017, **29**, 1605408; A. P. H. J. Schenning and E. W. Meijer, *Chem. Commun.*, 2005, 3245–3258.

3 A. Jain and S. J. George, *Mater. Today*, 2015, **18**, 206–214.

4 E. Lee, J. K. Kim and M. Lee, *Angew. Chem., Int. Ed.*, 2009, **48**, 3657–3660; X. Liu, X. Zhou, B. Shen, Y. Kim, H. Wang, W. Pan, J. Kim and M. Lee, *J. Am. Chem. Soc.*, 2020, **142**(4), 1904–1910; Z. Chen, Y.-T. Chan, D. Miyajima, T. Kajitani, A. Kosaka, T. Fukushima, J. M. Lobez and T. Aida, *Nat. Commun.*, 2016, **7**, 13640; Z. Lin, J. Sun, Y. Zhou, Y. Wang, H. Xu, X. Yang, H. Su, H. Cui, T. Aida, W. Zhang and S. Z. D. Cheng, *J. Am. Chem. Soc.*, 2017, **139**, 5883–5889; D. Sahoo, M. Peterca, E. Aqad, B. E. Partridge, P. A. Heiney, R. Graf, H. W. Spiess, X. Zeng and V. Percec, *J. Am. Chem. Soc.*, 2016, **138**, 14798–14807; Y. Kim, S. Shin, T. Kim, D. Lee, C. Seok and M. Lee, *Angew. Chem., Int. Ed.*, 2013, **52**, 6426–6429; J. del Barrio, J. Liu, R. A. Brady, C. S. Y. Tan, S. Chiodini, M. Ricci, R. Fernández-Leiro, C.-J. Tsai, P. Vasileiadi, L. Di Michele, D. Lairez, C. Toprakcioglu and O. A. Scherman, *J. Am. Chem. Soc.*, 2019, **141**, 14021–14025; B. Narayan, S. P. Senanayak, A. Jain, K. S. Narayan and S. J. George, *Adv. Funct. Mater.*, 2013, **23**, 3053–3060; K. Liu, Y. Yao, C. Wang, Y. Liu, Z. Li and X. Zhang, *Chem.–Eur. J.*, 2012, **18**, 8622–8628.

5 T. Fukui, S. Kawai, S. Fujinuma, Y. Matsushita, T. Yasuda, T. Sakurai, S. Seki, M. Takeuchi and K. Sugiyasu, *Nat. Chem.*, 2017, **9**, 493–499; N. Sasaki, J. Yuan, T. Fukui, M. Takeuchi and K. Sugiyasu, *Chem.–Eur. J.*, 2020, **26**, 7840–7846; D. S. Pal and S. Ghosh, *Chem.–Eur. J.*, 2018, **24**, 8519–8523.

6 J. B. Gilroy, T. Gädt, G. R. Whittell, L. Chabanne, J. M. Mitchels, R. M. Richardson, M. A. Winnik and I. Manners, *Nat. Chem.*, 2010, **2**, 566; S. H. Jung, D. Bochicchio, G. M. Pavan, M. Takeuchi and K. Sugiyasu, *J. Am. Chem. Soc.*, 2018, **140**, 10570–10577; X. He, M.-S. Hsiao, C. E. Boott, R. L. Harniman, A. Nazemi, X. Li, M. A. Winnik and I. Manners, *Nat. Mater.*, 2017, **16**, 481.

7 Z. M. Hudson, C. E. Boott, M. E. Robinson, P. A. Rupar, M. A. Winnik and I. Manners, *Nat. Chem.*, 2014, **6**, 893–898; X. He, Y. He, M. S. Hsiao, R. L. Harniman, S. Pearce, M. A. Winnik and I. Manners, *J. Am. Chem. Soc.*, 2017, **139**, 9221–9228.

8 D. van der Zwaag, T. F. A. de Greef and E. W. Meijer, *Angew. Chem., Int. Ed.*, 2015, **54**, 8334–8336; M. Wehner and F. Würthner, *Nat. Rev. Chem.*, 2019, **4**, 38–53; R. D. Mukhopadhyay and A. Ajayaghosh, *Science*, 2015, **349**, 241–242; A. Sorrenti, J. Leira-Iglesias, A. J. Markvoort, T. F. A. de Greef and T. M. Hermans, *Chem. Soc. Rev.*, 2017, **46**, 5476–5490.

9 S. Dhiman and S. J. George, *Bull. Chem. Soc. Jpn.*, 2018, **91**, 687–699; T. Fukui, N. Sasaki, M. Takeuchi and K. Sugiyasu, *Chem. Sci.*, 2019, **10**, 6770–6776; J. Matern, Y. Dorca, L. Sánchez and G. Fernandez, *Angew. Chem., Int. Ed.*, 2019, **58**, 16730–16740; G. Ghosh, P. Dey and S. Ghosh, *Chem. Commun.*, 2020, **56**, 6757–6769; M. Hartlieb, E. D. H. Mansfield and S. Perrier, *Polym. Chem.*, 2014, **11**, 1083–1110.

10 S. Ogi, V. Stepanenko, K. Sugiyasu, M. Takeuchi and F. Würthner, *J. Am. Chem. Soc.*, 2015, **137**, 3300–3307; S. Ogi, V. Stepanenko, J. Thein and F. Würthner, *J. Am. Chem. Soc.*, 2016, **138**, 670–678.

11 J. Kang, D. Miyajima, T. Mori, Y. Inoue, Y. Itoh and T. Aida, *Science*, 2015, **347**, 646–651.

12 S. Ogi, K. Sugiyasu, S. Manna, S. Samitsu and M. Takeuchi, *Nat. Chem.*, 2014, **6**, 188–195.

13 P. A. Korevaar, S. J. George, A. J. Markvoort, M. M. J. Smulders, P. A. J. Hilbers, A. P. H. J. Schenning, T. F. A. De Greef and E. W. Meijer, *Nature*, 2012, **481**, 492–496; P. A. Korevaar, T. F. A. de Greef and E. W. Meijer, *Chem. Mater.*, 2014, **26**, 576–586; J. Matern, K. K. Kartha, L. Sánchez and G. Fernandez, *Chem. Sci.*, 2020, **11**, 6780–6788.

14 T. Fukui, S. Kawai, S. Fujinuma, Y. Matsushita, T. Yasuda, T. Sakurai, S. Seki, M. Takeuchi and K. Sugiyasu, *Nat. Chem.*, 2017, **9**, 493–499.

15 S. Dhiman, A. Sarkar and S. J. George, *RSC Adv.*, 2018, **8**, 18913–18925; S. Dhiman and S. J. George, in *Advances in the Chemistry and Physics of Materials*, ed. S. J. George, C. Narayana and C. N. R. Rao, World Scientific, 2019, pp. 123–147.

16 A. Mishra, D. B. Korlepara, M. Kumar, A. Jain, N. Jonnalagadda, K. K. Bejagam, S. Balasubramanian and S. J. George, *Nat. Commun.*, 2018, **9**, 1295; A. Mishra, D. B. Korlepara, S. Balasubramanian and S. J. George, *Chem. Commun.*, 2020, **56**, 1505–1508; L. J. Iglesias, A. Sorrenti, A. Sato, P. A. Dunne and T. M. Hermans, *Chem. Commun.*, 2016, **52**, 9009–9012.

17 A. Jain, S. Dhiman, A. Dhayani, P. K. Vemula and S. J. George, *Nat. Commun.*, 2019, **10**, 450.

18 A. A. Sagade, K. V. Rao, U. Mogera, S. J. George, A. Datta and G. U. Kulkarni, *Adv. Mater.*, 2013, **25**, 559–564; X. Zhang and C. Wang, *Chem. Soc. Rev.*, 2011, **40**, 94–101; C. Wang, Y. Guo, Y. Wang, H. Xu, R. Wang and X. Zhang, *Angew. Chem., Int. Ed.*, 2009, **48**, 8962–8965; K. Liu, C. Wang, Z. Li and X. Zhang, *Angew. Chem., Int. Ed.*, 2011, **50**, 4952–4956; M. Kumar, K. V. Rao and S. J. George, *Phys. Chem. Chem. Phys.*, 2014, **16**, 1300–1303; K. Jalani, S. Dhiman, A. Jain and S. J. George, *Chem. Sci.*, 2017, **8**, 6030–6036; B. V. V. S. P. Kumar, K. V. Rao, T. Soumya, S. J. George and M. Eswaramoorthy, *J. Am. Chem. Soc.*, 2013, **135**, 10902–10905; A. Das and S. Ghosh, *Angew. Chem., Int. Ed.*, 2014, **53**, 2038–2054.

19 B. Kemper, L. Zengerling, D. Spitzer, R. Otter, T. Bauer and P. Besenius, *J. Am. Chem. Soc.*, 2018, **140**, 534–537; H. Frisch, E.-C. Fritz, F. Stricker, L. Schmüser, D. Spitzer, T. Weidner, B. J. Ravoo and P. Besenius, *Angew. Chem., Int. Ed.*, 2016, **55**, 7242–7246; J. P. Wojciechowski, A. D. Martin and P. Thordarson, *J. Am. Chem. Soc.*, 2018, **140**, 2869–2874.

20 R. Nguyen, L. Allouche, E. Buhler and N. Giuseppone, *Angew. Chem., Int. Ed.*, 2009, **48**, 1093–1096; Y. Kang, K. Liu and X. Zhang, *Langmuir*, 2014, **30**, 5989–6001; C. B. Minkenberg, L. Florusse, R. Eelkema, G. J. M. Koper and J. H. van Esch, *J. Am. Chem. Soc.*, 2009, **131**, 11274–11275; C. Wang, G. Wang, Z. Wang and X. Zhang, *Chem.–Eur. J.*, 2011, **17**, 3322–3325.

21 C. Tanford, *J. Phys. Chem.*, 1972, **76**, 3020–3024.

22 A. Sarkar, R. Sasmal, C. Empereur-Mot, D. Bochicchio, S. V. K. Kompella, K. Sharma, S. Dhiman, S. Balasubramanian, S. S. Agasti, G. M. Pavan and S. J. George, *J. Am. Chem. Soc.*, 2020, **142**, 7606–7617.